npj | computational materials

Article

Published in partnership with the Shanghai Institute of Ceramics of the Chinese Academy of Sciences

https://doi.org/10.1038/s41524-025-01868-z

Unified fracture criterion for brittle 2D materials

Shenda Jiang[1,3], Israel Greenfeld[2,3], Lin Yang[1] ✉, Weilong Yin[1], Xiaodong He[1] & H. Daniel Wagner[2] ✉

Two-dimensional materials (2DMs), possessing atomic-scale thickness, are prone to brittle fracture under loading conditions, which can lead to catastrophic failure. As their structural dimensions approach the nanoscale, conventional linear elastic fracture mechanics (LEFM) based on continuum assumptions is deficient in capturing the underlying failure mechanisms and accurately predicting potential crack instability. This limitation emphasizes the critical need for a new theoretical approach suited to the fracture behavior of 2DM systems. We propose a unified fracture mechanics (UFM) criterion that systematically incorporates two key physical mechanisms governing brittle fracture in 2DMs at the nanoscale, namely nonlinear elasticity and atomic-scale discreteness. By introducing two corrective parameters, for nonlinearity and quantization, the UFM model successfully resolves the limitations of LEFM in predicting failure. This is particularly important in the short crack regime, as small defects are frequent in 2DMs. The theoretical predictions show excellent agreement with molecular dynamics simulations of five different types of 2DMs and accurately capture the fracture strength of both cracked and defect-free structures. In addition, we present an empirical method that allows the fracture behavior of 2DMs to be estimated directly from their intrinsic structural and elastic properties. The unified theoretical framework is applicable not only to the materials simulated in this study but may also be applied to a broader class of atomically thin brittle systems.

Atomically thin two-dimensional materials (2D materials, 2DMs) exhibit outstanding mechanical, electrical, and thermal properties, and hold great promise for applications in nanoelectronic devices, energy storage, and nanocomposites[1–3]. However, the low fracture toughness of representative 2DMs limits their reliability during fabrication, transfer, and practical use, making them vulnerable to catastrophic failure under external mechanical loads. This inherent brittleness primarily stems from the nucleation and propagation of atomic-scale defects, such as vacancies, cracks, and voids, which eventually lead to brittle fracture[4–6]. Therefore, a comprehensive understanding of the fracture mechanisms of defective, brittle 2DMs at the nanoscale is essential for the design and manufacturing of reliable nanodevices.

In recent years, researchers have systematically investigated the fracture behavior of brittle 2DMs at atomic resolution using in situ experiments and theoretical simulations, revealing their unique fracture mechanisms. Among these studies, the theoretical framework of classic linear elastic fracture mechanics (LEFM) has been widely used to predict and analyze the fracture toughness of such materials[7–12]. However, multiple experimental and simulation-based investigations have shown that the fracture behavior of typical brittle 2DMs at the nanoscale deviates significantly from the predictions of LEFM[10,13–20]. This deviation arises mainly due to atomic-scale discreteness and anisotropy, non-uniform stress fields, and the nonlinear nature of interatomic interactions[10,14,16,20]. In this context, developing a mechanical model that accurately incorporates the physical mechanisms of brittle fracture at the atomic scale becomes a critical issue.

To overcome the limitations of LEFM at the nanoscale, several modified fracture theories have been proposed. For example, quantized fracture mechanics (QFM) and atomic fracture mechanics (AFM) introduce atomic-scale discreteness and provide a framework for describing fracture in small-scale discrete systems[16,19,21]. However, brittle fracture in 2DMs exhibits pronounced nonlinearity at the atomic scale, and fracture criteria based solely on discreteness are insufficient to capture their intrinsic fracture mechanisms[10]. Recently, a theoretical model combining nonlinear elasticity and atomic discreteness was developed to successfully describe the fracture behavior of monolayer MXene[20]. Nevertheless, a unified fracture criterion capable of capturing the fundamental nature of brittle fracture in 2DMs at the nanoscale, and

[1]National Key Laboratory of Science and Technology on Advanced Composites in Special Environments, Center for Composite Materials and Structures, Harbin Institute of Technology, Harbin, China. [2]Department of Molecular Chemistry and Materials Science, Weizmann Institute of Science, Rehovot, Israel. [3]These authors contributed equally: Shenda Jiang, Israel Greenfeld. ✉e-mail: Linyang@hit.edu.cn; Daniel.Wagner@weizmann.ac.il

applicable to fracture toughness prediction across scales from the nanoscale to the macroscale, has yet to be established.

In this work, we perform molecular dynamics simulations on four representative brittle 2DMs, including graphene, hexagonal boron nitride (h-BN), molybdenum disulfide (MoS_2), and Titanium carbide MXene (Ti_3C_2), and propose a cross-scale unified fracture model (UFM) that incorporates nonlinear elasticity and atomic discreteness. For completeness, the analysis results of Ti_2C, which we previously studied and published in ref. 20, are also presented. We define representative slit defects, ranging from single to many atomic vacancies, and simulate them by applying uniaxial tension and recording their far-field stress at failure. The UFM model is fitted to the simulation results, allowing prediction of the strength of flawed 2DMs, offering a universal approach. The model is extended for predicting the stress concentration at crack tips, as well as the pristine strength of flawless 2DMs, both unattainable from LEFM. Also offered is prediction for future 2DMs, based solely on their structural and elastic properties. The material resistance to crack propagation and crack instability are analyzed using the J-integral method. The simulation and modeling align excellently, and are compared with 2DMs studies published in the literature.

Materials and methods

To investigate the fracture behavior of monolayer brittle 2DMs containing pre-existing cracks at the nanoscale, we performed large-scale molecular dynamics (MD) simulations using the Large-scale Atomic/Molecular Massively Parallel Simulator (LAMMPS)[22]. Four representative brittle 2DMs, extensively studied in recent literature, were selected: graphene, h-BN, MoS_2, and Ti_3C_2. The crystal structures of the four monolayer 2DMs investigated in this study are illustrated in Fig. 1. Graphene consists of a two-dimensional hexagonal honeycomb lattice of carbon atoms, where each atom forms three strong covalent bonds through sp^2 hybridization[23]. Hexagonal boron nitride (h-BN) has a similar lattice, with alternating boron (B) and nitrogen (N) atoms, and exhibits pronounced polarity in its B–N bonds[24]. Monolayer MoS_2 adopts a stable 2H phase with a characteristic sandwich-like structure, in which a layer of molybdenum (Mo) atoms is sandwiched between two layers of sulfur (S) atoms, forming an S-Mo-S configuration[25]. Ti_3C_2 MXene features a hexagonal close-packed (HCP) crystal structure, where Ti atoms are arranged in a dense stacking, and C atoms occupy the octahedral sites between Ti layers[26]. The unit structure consists of five atomic layers stacked in a Ti-C-Ti-C-Ti sequence, highlighting its layered nature.

The fracture behavior of these 2DMs was modeled using well-established interatomic potentials: the AIREBO potential for graphene[27], the Tersoff potential for h-BN[28], the REBO potential for MoS_2[29], and the ReaxFF potential for Ti_3C_2[30]. Previous MD studies have demonstrated that these potentials are capable of reliably capturing the mechanical response and fracture characteristics of the corresponding materials[16,31–33]. The applicability of these force fields in modeling the mechanical properties of 2DMs is systematically validated in Section S1 of the SI (The stress–strain comparisons are shown in Fig. S1, and the parameter settings of the MoS_2 REBO potential are listed in Table S1.). Their predictive accuracy was further assessed by comparing with benchmark results from density functional theory (DFT) calculations reported in the literature. Further details of the simulation procedures can be found in Section S2 of the SI.

Results and discussion

Crack size and brittle fracture

Figure 2 illustrates the simulation setup for anisotropic brittle 2D materials (2DMs) under uniaxial tensile loading with a central slit crack. Given the pronounced lattice anisotropy of 2DMs, simulations were conducted along both the zigzag (ZZ) and armchair (AC) directions. Ideal straight pre-cracks were introduced by sequentially removing atomic rows perpendicular to the loading direction, and the specific sequence details are provided in Section S3.3. Specifically, armchair-oriented defects were loaded along the zigzag direction, and zigzag-oriented defects were loaded along the armchair direction. Although in reality defects in 2DMs are not purely shaped as straight slits, this configuration allows comparison with an explicit theoretical model that yields the intrinsic fracture toughness of these materials.

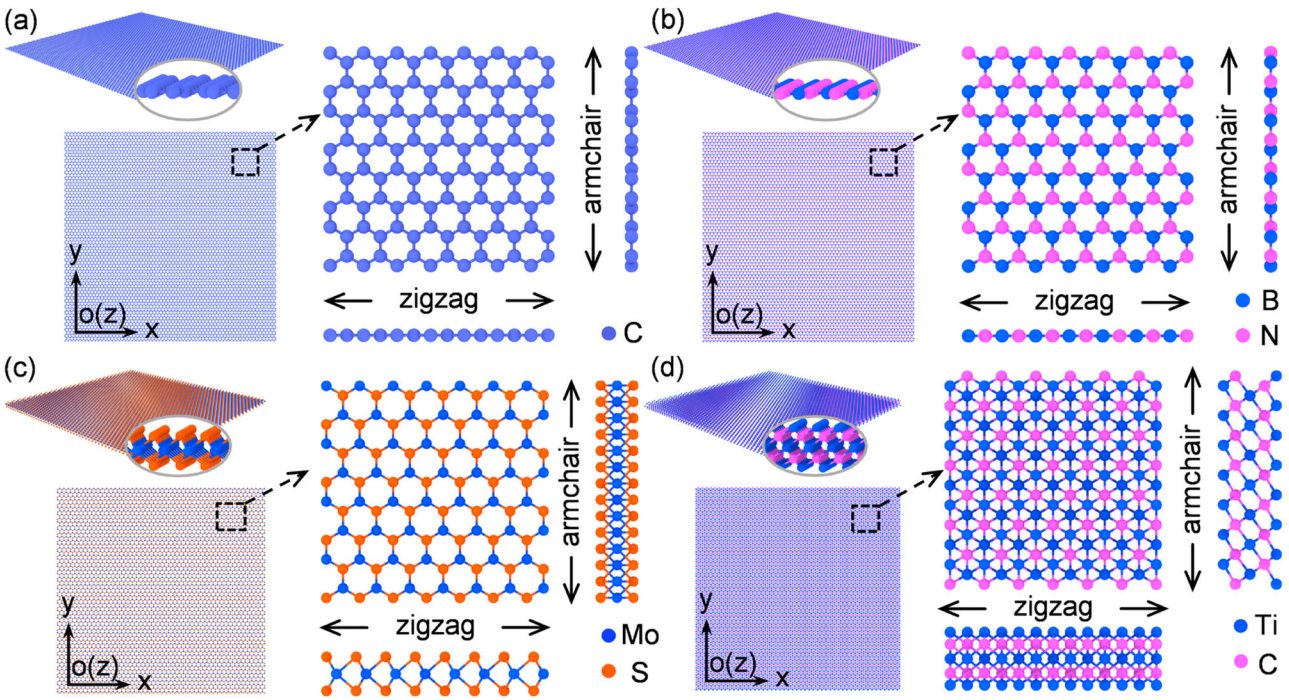

Fig. 1 | Atomic structures of four representative 2D materials. a Graphene, **b** hexagonal boron nitride (h-BN), **c** molybdenum disulfide (MoS_2), and **d** Ti_3C_2 MXene. The 2DMs exhibit hexagonal structures, with graphene and h-BN consisting of a single planar atomic layer, whereas MoS_2 and Ti_3C_2 have 3 or 5 layers, respectively.

To accurately apply fracture mechanics theory to brittle 2DMs, it is essential to establish a quantitative relationship between fracture toughness, applied stress, and crack length. However, due to the atomic discreteness of 2DMs, the conventional continuum definition of crack length fails to capture the true physical dimension of atomic-scale cracks, especially for short cracks. Therefore, we introduce a unified and quantifiable definition of the crack length $2a$. As shown in Fig. 3a–d, detailed analysis of lattice parameters and crack geometry reveals that the crack length is essentially a discrete function of the number of missing atoms. Based on this, the analytical expressions for the crack length $2a$ as a function of the number of removed atoms N_v for all four studied 2DMs are derived and provided in Section S3 of the SI. These functions ensure convergence to null length ($2a = 0$) when no atoms are removed (pristine material).

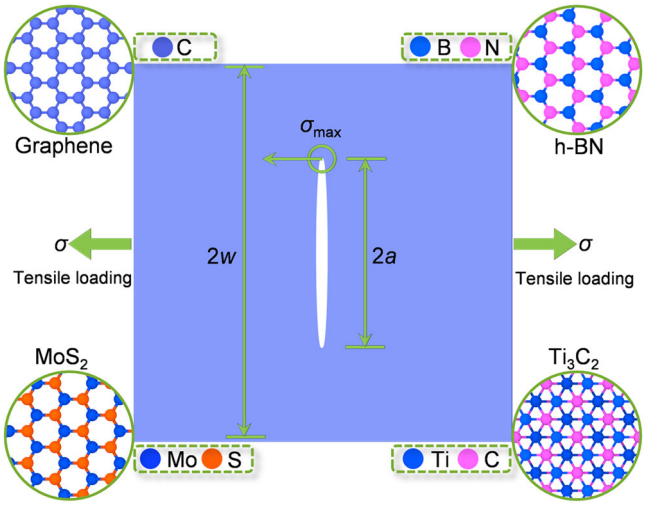

Fig. 2 | Schematic illustration of the tensile loading setup. Cracked model of four representative 2DMs under uniaxial tension. Here, σ denotes the applied far-field stress, σ_{max} is the maximum stress at the crack tip, $2w$ is the width of the monolayer, and $2a$ represents the crack length. Using a slit defect in the MD simulation enables comparison with known theoretical models.

Based on the discrete function definitions of crack length, we further constructed a series of numerical models containing pre-existing cracks of varying orientations and sizes. These models were used to systematically investigate the fracture response of 2DMs under the combined effects of nonlinear elasticity and atomic-scale discreteness, and to provide quantitative parameters for the development of a UFM model. Figure 4a–b shows the pre-cracked configurations of graphene and Ti_3C_2 with cracks aligned along the armchair and zigzag directions, respectively. Since the modeling procedures for h-BN and MoS_2 are analogous to that of graphene, their geometric structures are provided separately in Fig. S2 of the SI to maintain visual clarity.

Due to computational limitations associated with the ReaxFF potential, the maximum width of the Ti_3C_2 model was set to 148 nm, consistent with a previous study[20]. For the remaining three 2DMs, the maximum model width was approximately 200 nm. To eliminate size effects on the simulation results, all models were constructed such that the total sample width ($2w$) was at least ten times larger than the crack length ($2a$).

Figure 5a–d presents the stress evolution and crack propagation behavior in zigzag-oriented defective models of four representative 2DMs, each containing a central crack and subjected to uniaxial tensile loading. The selected models include ZZ 113 C (graphene), ZZ 56B57N

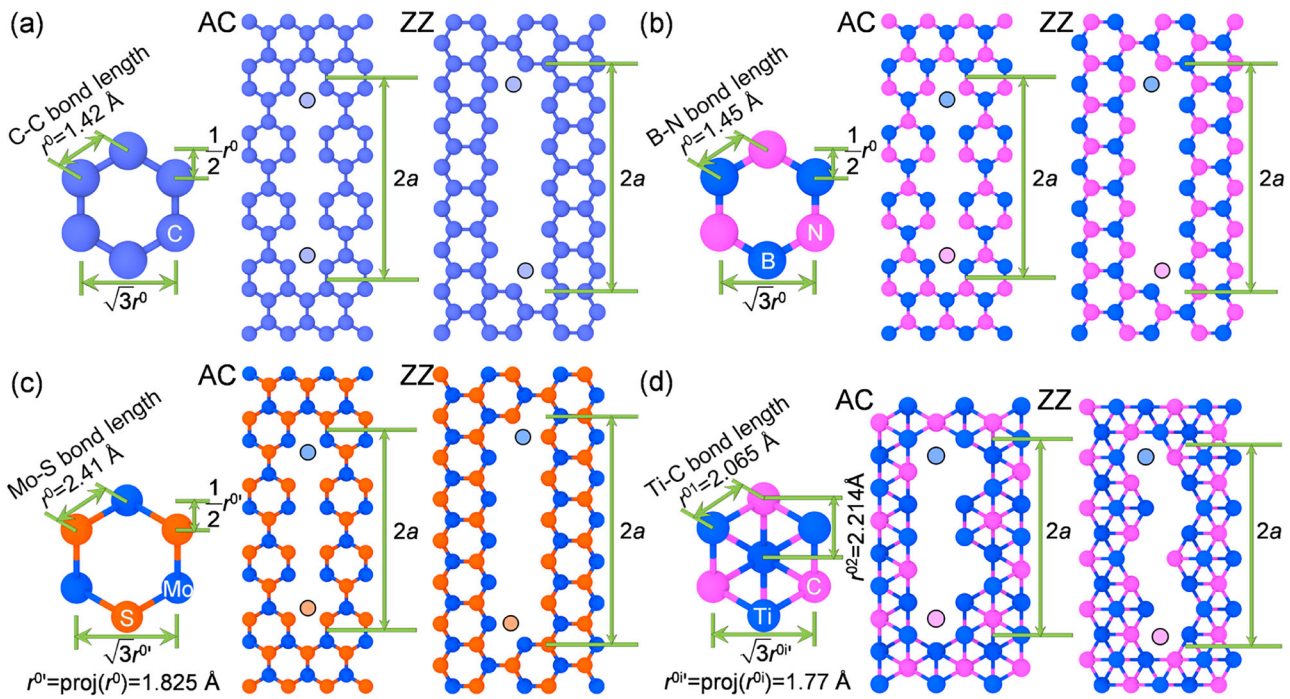

Fig. 3 | Definition of crack length. Lattice geometry with removed atoms and crack length definitions for **a** graphene, **b** h-BN, **c** MoS_2, and **d** Ti_3C_2, for armchair (AC) and zigzag (ZZ) oriented defects. The unbonded atoms are the missing atoms closest to the crack tips. Based on these definitions, crack length may be expressed as function of the number of missing atoms.

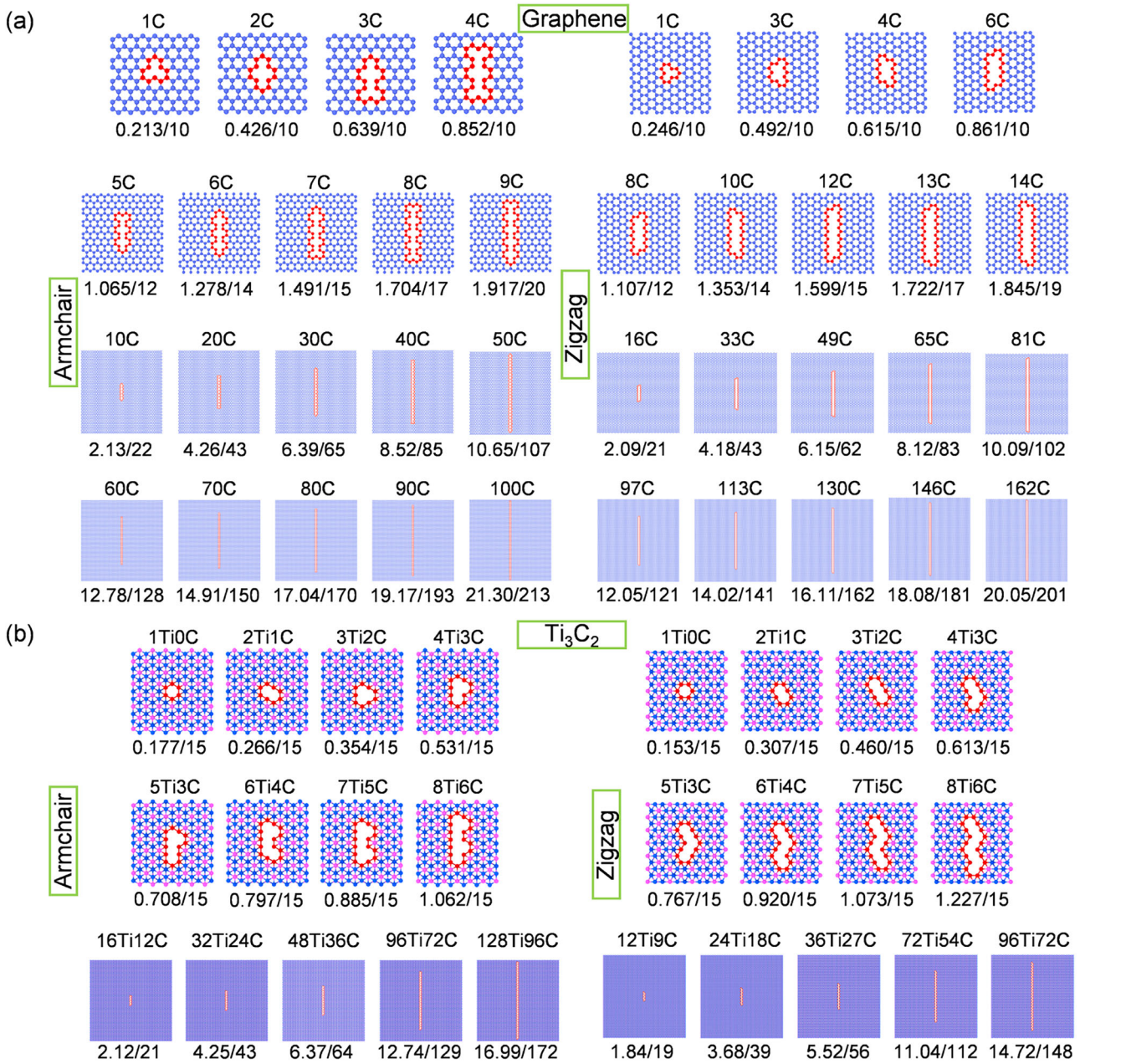

Fig. 4 | Central pre-cracked structures. Cracked models of **a** graphene and **b** Ti_3C_2. The number and type of missing atoms is indicated above each configuration, while the crack-to-width ratio ($2a/2w$) is labeled below. To clearly visualize the slit crack, only the central region containing the crack is shown here, while the full simulation model is larger in size.

(h-BN), ZZ 44Mo88S (MoS_2), and ZZ 96Ti72C (Ti_3C_2), all with an initial crack length of approximately 14 nm. Upon applying far-field stress perpendicular to the crack direction, strong stress concentration arises at the crack tips. When the local stress exceeds the bond strength of the material, covalent bonds at the crack front rupture abruptly, initiating crack growth. This process characterizes a typical brittle failure mechanism. Following crack propagation, the high-stress region remains localized at the crack tip until complete structural failure occurs. The blue, low-stressed areas are regions whose strain energy was released by crack growth.

Unified fracture criterion

Based on the typical brittle failure characteristics observed during crack propagation in the above atomistic simulations of four 2D materials, this study establishes a unified fracture mechanics criterion to describe their fracture behavior. This criterion introduces adaptations for nonlinearity and quantization to fracture mechanics. Modeling details are provided in Section S4 in the SI.

Characteristics of 2D materials. Atomically thin 2DMs possess two characteristic properties: (i) Their structure consists of atoms connected by covalent bonds, and therefore, unlike continuum solids, it is discrete; (ii) They remain elastic under load all the way until fracture, in other words, they are brittle materials. Furthermore, their elasticity is nonlinear, most likely due to residual stresses in their atomic structure at equilibrium state[20]. Both properties impact the 2DM fracture behavior, and so we start by defining these properties in a way usable in fracture modeling.

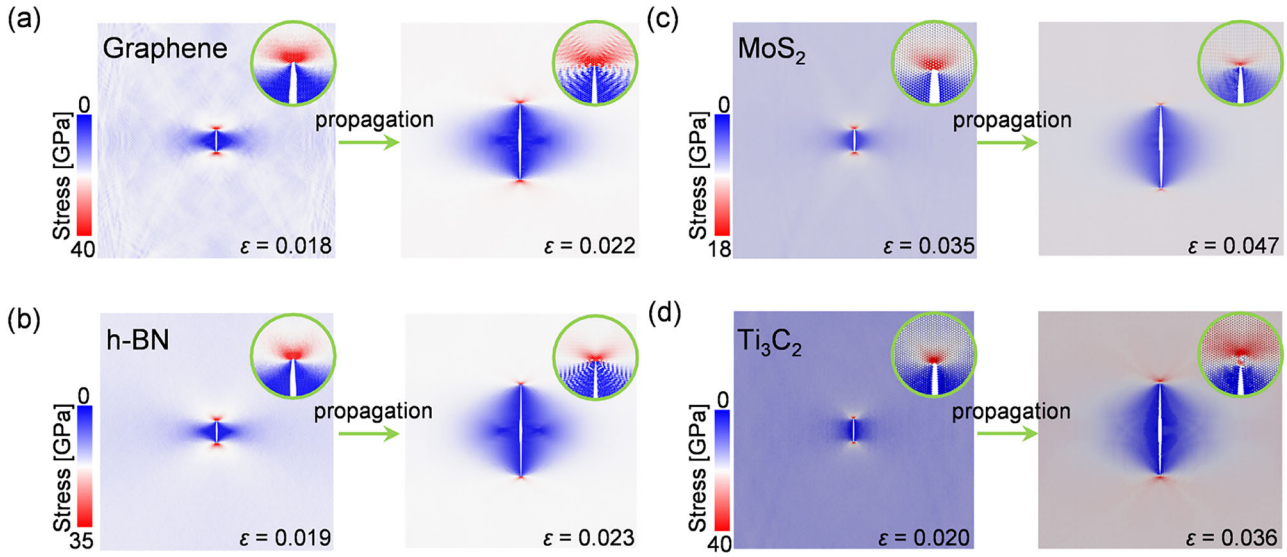

Fig. 5 | Stress concentration and crack propagation. Stress contour plots of four 2DMs: **a** graphene, **b** h-BN, **c** MoS_2, and **d** Ti_3C_2, each with a centrally pre-cracked configuration along the zigzag direction (initial crack length ~ 14 nm). Left panels show stress concentration at the moment of crack initiation, and right panels illustrate stress evolution during spontaneous crack propagation under continued tensile loading. Insets provide a magnified view of stress concentration at the crack tips. The red spots indicate stress concentration at crack edges; the blue regions represent relieved strain.

The effect of discreteness on fracture is reflected in the way a crack propagates in an atomic structure by progressively breaking bonds and/or removing atoms. Thus, the crack advances in discrete steps, which may be expressed by a fracture quantum[20,34]:

$$q \cong \frac{2a}{m(N_v)} \tag{1}$$

where $2a$ is the length of a slit crack, N_v is the number of atomic vacancies forming the crack. and $m(N_v)$ is the number of discrete advancement steps of crack growth (see Sections S3.1 and S4.3 of the SI for details; see Table S2 in Section S4.3). The limit values for long cracks are $q_{AC} \cong \frac{3}{4}r$ and $q_{ZZ} \cong \frac{\sqrt{3}}{2}r$, where r is the projection of the bond length on the 2DM plane (Fig. 3).

The effect of material nonlinearity is commonly expressed by the empirical Ramberg-Osgood (RO) Equation[35,36], where the strain ε is a nonlinear function of the stress σ. RO is used here in the following form[20]:

$$\varepsilon = \frac{\sigma}{E}\left[1 + \left(\frac{\sigma}{\sigma_0}\right)^{n-1}\right] \tag{2}$$

with E the elastic modulus (slope at the origin of the stress-strain curve), σ_0 a reference stress, and n a strain hardening/softening exponent. The nonlinearity is determined by the parameters σ_0 and n. The independent parameters, E, σ_0 and n, are obtained by fitting this equation to the stress-strain curves of each material, as obtained by molecular dynamics and density functional theory (DFT) calculations (refer to Section S5 and Fig. S3 in the SI). As RO was originally developed for metals and plastic behavior, it is not optimized for 2DMs and overestimates the stress in the high strain regions. However, as will be shown, this causes only minor deviations in the 2DMs fracture model. In addition to the elastic properties, the MD analysis of the pristine, defect-free material provides its ultimate strength, σ_u, the far-field stress at fracture.

Energy release rate and fracture stress. Fracture mechanics diverges from traditional strength-based approaches by emphasizing energy balance as the primary criterion for failure. When a crack propagates through a structure under load, it releases stored elastic energy, which drives the breaking of bonds along the crack path. This stored elastic energy is calculated by integrating the area under the stress-strain curve over a strained region around the crack, using the nonlinear model in Eq. (2). This energy becomes accessible upon crack initiation and propagation, and is expressed by J, the strain energy release rate per unit area of incremental crack extension. In addition, as the material structure is discrete, continuity of J is recovered by averaging it over the fracture quantum q defined in Eq. (1). The resulting energy release rate is given by:

$$J = \frac{\pi\sigma^2(a + q/2)}{E}\left[1 + \frac{h_1}{\pi}\left(\frac{\sigma}{\sigma_0}\right)^{n-1}\right] \tag{3}$$

assuming that the 2DMs width is much larger than the defect length[20,36,37]. h_1 is a dimensionless geometry correction factor for a center-cracked plate.

The defect length in this equation is augmented by $q/2$ as a result of the quantization, and the nonlinearity is expressed by the second term in the brackets. When cracks are very long (low fracture stresses), both these effects become negligible, and the classic LEFM model, $\sigma = \sqrt{JE/\pi a}$, is recovered. However, quantization and nonlinearity both have a major impact on toughness in the presence of short defects, because the energy released for driving a crack is larger than the energy in LEFM, with the consequence of reducing the toughness. The nonlinearity effect can be understood as follows: the stiffness at fracture under high stress (short defects) is lower compared to low stress conditions (long defects). This is reflected by the smaller slope of the stress-strain curve at high stress (see stress-strain plots in the SI, Fig. S1), leading to a higher elastic energy density, which correlates inversely with the stiffness. This nonlinearity effect becomes more pronounced

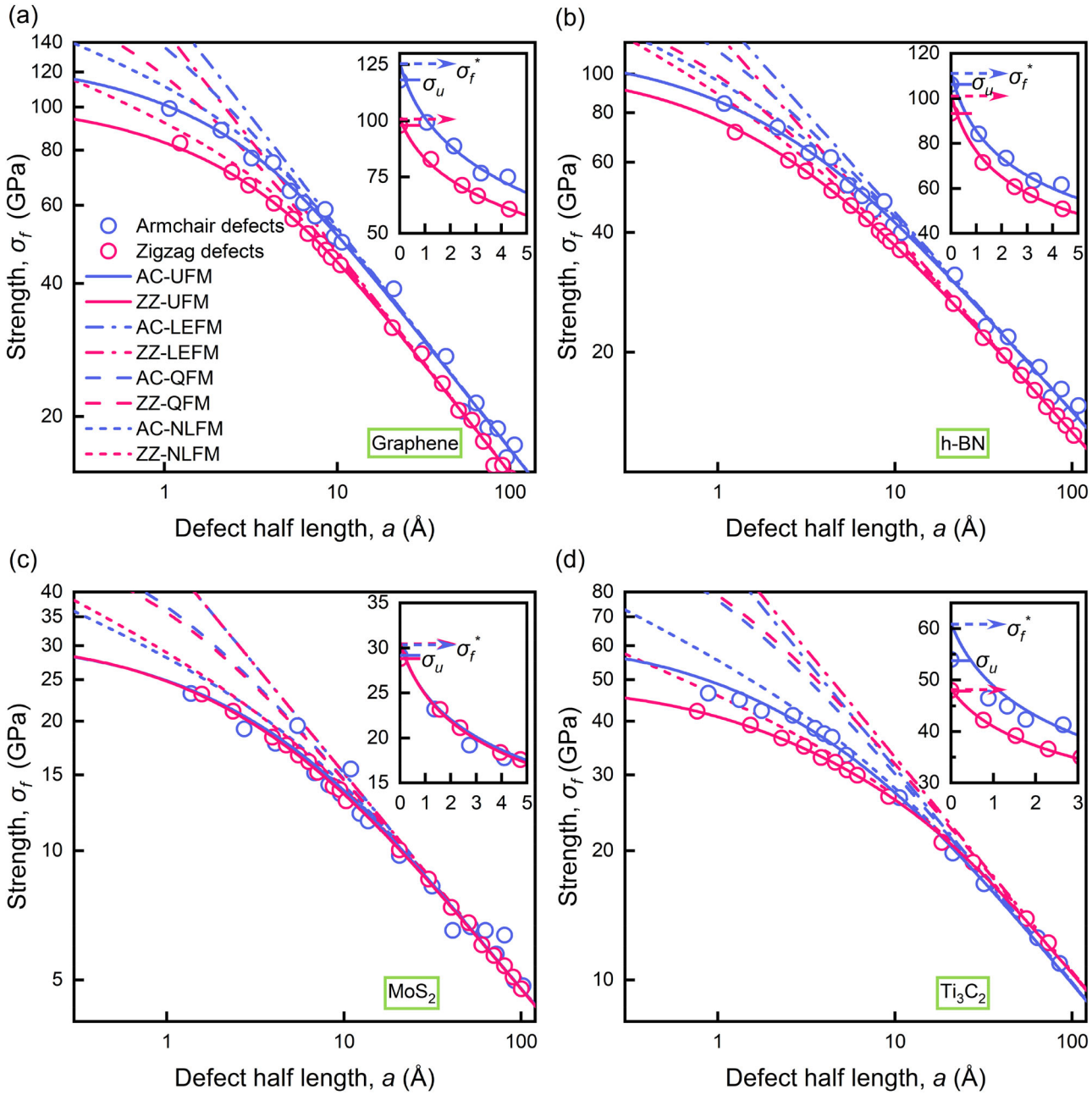

Fig. 6 | Simulated fracture strength and modeling. Log-log plots of the strength σ_f of armchair and zigzag defected models vs. the defect half-length a. Panels: **a** graphene, **b** h-BN, **c** MoS_2 and **d** Ti_3C_2. The theoretical trendlines of the unified model (UFM, Eq. (4)) are fitted to the simulation data; the basic linear model (LEFM) and the separate effects of the quantization (QFM) and nonlinearity (NLFM) models are also presented. Insets: magnified linear-linear plots showing the pristine strength predictions, σ_f^* (UFM model) and σ_u (MD simulation). Acronyms: UFM unified fracture mechanics, LEFM linear elastic fracture mechanics, QFM quantized fracture mechanics, NLFM nonlinear fracture mechanics. The UFM model fits excellently to the MD simulation datasets.

with increasing values of the ratio σ/σ_0, particularly at high stress levels.

Given the far-field fracture stress σ_f and the critical energy release rate J_{Ic}, the critical defect half-length is obtained by inverting Eq. (3):

$$a = \frac{EJ_{Ic}}{\pi\sigma_f^2\left[1+\frac{h_1}{\pi}\left(\frac{\sigma_f}{\sigma_0}\right)^{n-1}\right]} - \frac{q}{2} \tag{4}$$

where $\sqrt{EJ_{Ic}} = K_{Ic}$, the fracture toughness. This is the *unified fracture criterion*, which is in excellent agreement with the MD fracture data of the materials in this study (Fig. 6 and Fig. S4, quality of fit $R^2 > 0.999$; Ti_2C simulation data from a previously published study[20].). The parameters J_{Ic} and h_1 were obtained by fitting to the MD fracture data, given q, E, σ_0 and n obtained by Eqs. (1) and (2) for each material (see Table 1). Due to the brittle behavior of the studied materials, J_{Ic} is constant for each of them, regardless of defect size (see ahead).

Table 1 | Summary of molecular dynamics simulations of defect-free and defected 2D materials

2DMs	Defect Type	Defect-free properties[a]				Defected fracture properties[b]							
		E GPa	σ_0 GPa	n -	σ_u GPa	σ_f^* GPa	K_{Ic} MPa m$^{0.5}$	J_{Ic} J m^{-2}	h_1 -	k -	q Å	p Å	a^* Å
Graphene	AC	792	130	5.89	118	120	3.00	11.37	8.61	0.53	1.07	1.76	2.29
	ZZ	939	114	5.73	98	99	2.65	7.48	14.15	0.59	1.23	1.91	2.53
h-BN	AC	709	115	4.40	106	106	2.52	8.96	6.90	0.51	1.09	1.33	1.88
	ZZ	744	118	3.71	93	93	2.24	6.74	6.81	0.68	1.26	1.25	1.88
MoS_2	AC	140	32	4.77	29	29	0.85	5.16	9.70	0.58	1.37	2.28	2.97
	ZZ	152	37	4.14	29	29	0.85	4.76	12.07	0.74	1.58	2.02	2.81
Ti_3C_2	AC	454	62	4.19	54	53	1.75	6.75	9.74	0.69	1.33	2.98	3.65
	ZZ	470	56	4.92	48	46	1.85	7.29	28.78	0.74	1.53	3.78	4.55
Ti_2C	AC	555	78	4.08	59	57	1.68	5.08	24.00	0.85	1.33	1.75	2.42
	ZZ	543	88	3.79	61	59	1.75	5.64	27.99	0.90	1.54	1.43	2.20

[a]Definition of parameters: fit to defect-free stress-strain simulation;
[b]Definition of parameters: fit to defected fracture simulation.

E elastic modulus at low strain (Eq. (2))	J_{Ic} critical energy release rate (Eq. (4))
σ_0 reference stress (Eq. (2))	h_1 geometry factor center-cracked plate (Eq. (4))
n strain hardening/softening exponent (Eq. (2))	q fracture quantum (Eq. (1))
σ_u ultimate strength	k fitting factor (Eq. (6))
σ_f^* defect-free strength (Eq. (8))	p nonlinearity parameter (Eq. (5))
K_{Ic} fracture toughness (Eq. (4))	a^* nonlinearity-quantization parameter (Eq. (8))

Figures 6 and S4 show that the quantization (denoted QFM) and nonlinearity (denoted NLFM), each by itself, is not sufficient for describing the fracture stresses. Only the unification of both (denoted UFM), as outlined by Eq. (4), can explain the observed fracture behavior. We see that both nonlinearity and quantization tend to decrease the critical defect length, meaning that failure at a given stress might occur at smaller defects. Furthermore, the nonlinearity effect is dominant over that of quantization for the 2DMs in this study.

To obtain the fracture stress explicitly, Eq. (4) can be approximated by:

$$\sigma_f \cong \sqrt{\frac{EJ_{Ic}}{\pi\left(a+\frac{q}{2}+p\right)}} \tag{5}$$

where the nonlinearity parameter (length unit) is defined as:

$$p = \frac{2nk}{n+1}\frac{EJ_{Ic}}{\pi\sigma_0^2} \tag{6}$$

with k a dimensionless fitting parameter. The mathematical derivation of this approximation from Eq. (4) is presented in the SI, Section S4.6. These two equations provide an approximation for the *unified fracture criterion*, which fits very well the MD fracture data ($R^2 > 0.99$) (See Fig. S5 in the SI), and offer instructive insights: (i) The nonlinearity expresses itself by augmenting the defect length, in the same way as the quantization, possibly implying that its source is related to the structural discreteness; (ii) The nonlinearity parameter depends on the critical energy release rate J_{Ic} (in addition to the RO elastic parameters), implying a complex interdependence.

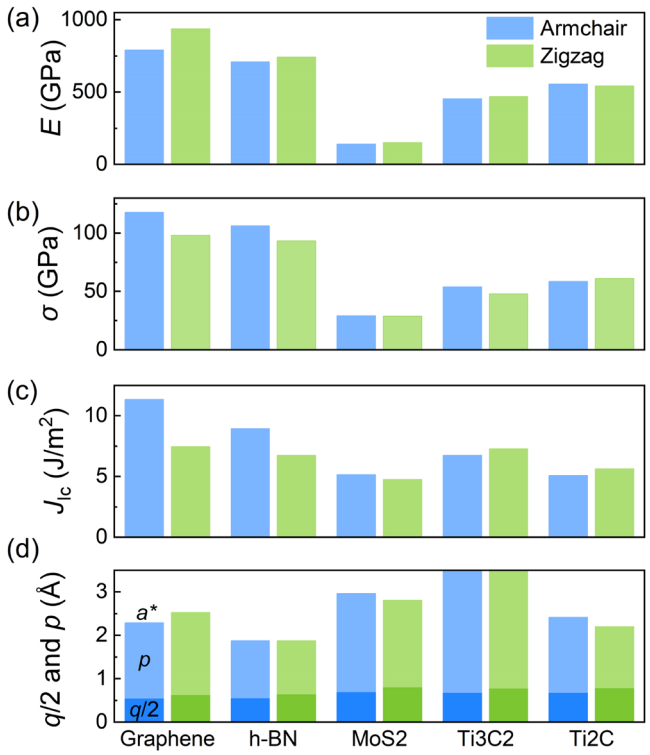

Fig. 7 | Main results of molecular dynamics simulations of 2DMs. a E the elastic modulus at low strain (Eq. (2)); **b** σ_u the ultimate strength; **c** J_{Ic} the critical energy release rate (Eq. (4)); **d** q the fracture quantum (quantization parameter) (Eq. (1)), p the nonlinearity parameter (Eq. (5)), and a^* the combined nonlinearity-quantization parameter (Eq. (8)). The planar single-layer 2DMs (graphene and h-BN) exhibit better stiffness, strength and toughness compared to the multilayer 2DMs.

The main results listed in Table 1 are depicted in Fig. 7, revealing basic trends. The key mechanical properties of the 2DMs are in correlation to each other, such that high modulus is associated with high ultimate strength and high energy release rate, and vice versa. Furthermore, high mechanical properties are generally associated with weaker nonlinearity (p) and lower quantization (q), and vice versa, as predicted by Eqs. (3)–(5). Smaller q reflects a shorter bond length, generally associated with high strength and

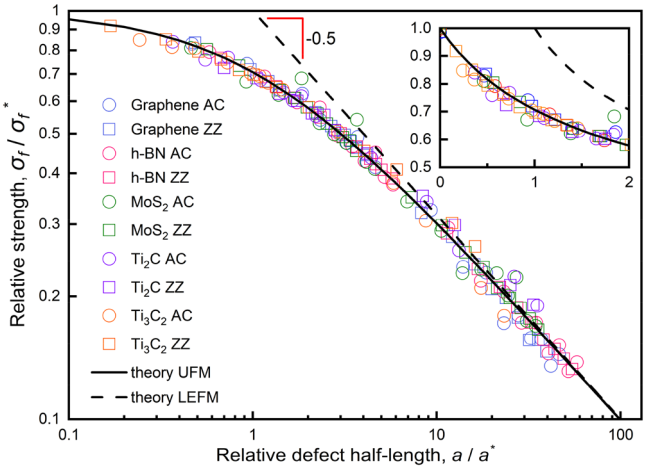

Fig. 8 | Simulated fracture strength—universal plot. Log-log plot of the strength σ_f of armchair (circles) and zigzag (squares) defected models vs. the defect half-length a, and theoretical trendlines (Eq. (9)). The five studied 2D materials are collapsed into a single plot by normalizing the strength by the defect-free strength σ_f^* and the defect half-length by the combined nonlinearity-quantization parameter a^* (values from Table 1). Inset: magnified linear-linear plot showing the pristine strength prediction, σ_f^*. Acronyms: UFM – unified fracture mechanics, LEFM – linear elastic fracture mechanics. This universal plot demonstrates that 2DMs share similar fracture behavior, and allows predictions for future 2DMs.

stiffness. Although the 2DMs are not in-plane isotropic, their performance in the armchair and zigzag directions is generally similar. The highest mechanical performance is exhibited by graphene, likely the result of its strong C-C bonds, compared to the bonds between two different elements in the other materials. The next high performance 2DM is h-BN, whose planar hexagonal structure and cell dimensions resemble graphene. By comparison, the MoS_2 and the MXenes have three-dimensional structures which are more likely to incur residual strains and prestresses which increase nonlinearity.

Pristine strength. Classic fracture mechanics has a major shortcoming in the limit of very small defects and defect-free structures, where its prediction for the strength σ_f^* diverges to infinity ($\sigma \sim 1/\sqrt{a}$). This is not the case when using the unified fracture criterion:

$$\sigma_f^{*2}\left[1+\frac{h_1}{\pi}\left(\frac{\sigma_f^*}{\sigma_0}\right)^{n-1}\right]=\frac{2EJ_{Ic}}{\pi q} \tag{7}$$

obtained from Eq. (4) with $a = 0$, or explicitly from the approximation in Eq. (5):

$$\sigma_f^* \cong \sqrt{\frac{EJ_{Ic}}{\pi a^*}} \cong \frac{K_{Ic}}{\sqrt{\pi a^*}}, \text{ where } a^* = p + q/2 \tag{8}$$

Thus, both nonlinearity and quantization reduce the defect-free strength. A more pronounced nonlinearity (small σ_0) will tend to decrease the defect-free strength. Using the fitting data, the prediction of the pristine strength σ_f^* is within 13% (Eq. (7)) and 4% (Eq. (8)) deviation from the ultimate strength σ_u obtained from the stress-strain simulation. Surprisingly, the approximate prediction (presented in Table 1) is tighter than the accurate prediction, possibly due to self-canceling errors. The parameter a^* is a material property that reflects the intrinsic nonlinearity (through p, Eq. (6)) and the atomic-scale discreteness (through q, Eq. (1)) of the 2DMs.

Combining Eqs. (5) and (8), we may form a normalized relationship for the fracture stress dependence on defect length:

$$\frac{\sigma_f}{\sigma_f^*} \cong \left(1+\frac{a}{a^*}\right)^{-1/2} \tag{9}$$

This theoretical prediction is presented in Fig. 8 along with the fracture data obtained by the MD defect simulations. In this plot, the fracture behavior of all the studied materials is collapsed into a single universal curve. Given a new, unstudied atomic layer material with pristine strength (predicted σ_f^* or simulated σ_u) and known nonlinearity-quantization parameter a^* — all material properties invariant with respect to shape and size — its fracture behavior in the presence of defects may be described by this equation and plot.

As noted, a^* is a material property encapsulating nonlinearity and quantization. For the studied 2DMs, nonlinearity dominates the influence on fracture toughness, particularly in structures with short defects (see Figs. 6 and 7d). Quantization effects, tied to atomic-scale cell size, become negligible at larger structural scales where $a \gg q$. In contrast, nonlinearity impacts fracture toughness across all scales. While nonlinearity alone still predicts divergent strength for vanishing cracks (Eq. (7) with $q = 0$), Eq. (8) mitigates this, despite being approximate. Ultimately, the combined nonlinearity-quantization framework yields accurate strength predictions for pristine 2DMs, as shown in Fig. 6 (insets).

As in the studied materials $p \gg q/2$ (Fig. 4d), an upper bound for the defect-free strength may be estimated by combining Eqs. (6) and (8):

$$\sigma_f^* \lesssim \sqrt{\frac{EJ_{Ic}}{\pi p}} = \sqrt{\frac{n+1}{2nk}}\sigma_0 \tag{10}$$

depending solely on the nonlinearity parameters n and σ_0. This estimate may apply to nonlinear bulk materials as well, where the quantization is negligible with respect to the size scale. Thus, the more linear a material's elastic response (large σ_0), the higher its pristine strength—and conversely, greater nonlinearity corresponds to lower strength. This is a notable result, linking the pristine strength of nonlinear elastic materials directly to their degree of nonlinearity. The underlying mechanism is likely the presence of residual stresses, which contribute simultaneously to elastic nonlinearity and to strength reduction, as elaborated in ref. 20.

Stress concentration. Fracture mechanics was originally developed to overcome the limitation of classical mechanics, which predicted, via stress concentration models[38,39], that the stress at the tip of a sharp crack would diverge to infinity. However, in the case of atomic layers like 2DMs, defects are never infinitesimally sharp, because an atom vacancy or a removed bond result in a defect edge that is not sharp. In fact, the defect edge is roughly round (more accurately, hexagonal, see Fig. 3), with a dimension that scales with the cell size. The stress concentration in a continuum solid with a defect that has round edges is modeled by the known Inglis model, $K_t = 1 + 2\sqrt{a/\rho}$, where ρ is the tip radius, using the equivalent-ellipse approximation[38,39]. As said, this prediction unrealistically diverges for sharp defects.

However, the tips of 2DM defects are neither circular nor sharp, making this prediction unsuitable for 2DMs[20]. Stress concentration is defined as the ratio between the stress at the defect tip and the applied far field stress. At fracture, this ratio is given by the maximum tip stress σ_{max} (Fig. 2) and the fracture stress σ_f, where σ_{max} may be estimated by the pristine strength σ_f^*. Thus:

$$K_t = \frac{\sigma_{max}}{\sigma_f} \cong \frac{\sigma_f^*}{\sigma_f} \cong \left(1+\frac{a}{a^*}\right)^{1/2} \tag{11}$$

where the term on the right was obtained by inverting Eq. (9). The vertical axis of Fig. 8 is in fact K_t^{-1}, attesting to the good agreement of this stress

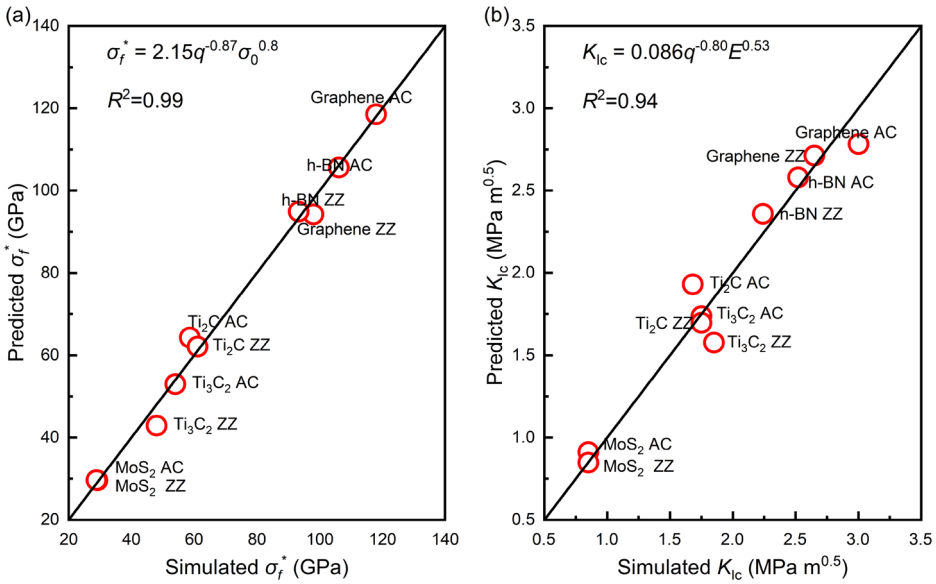

Fig. 9 | Predictions of pristine strength and fracture toughness vs. MD simulations. Two-variable power fits of **a** the pristine strength σ_f^* and **b** fracture toughness K_{Ic}. The independent variables are the fracture quantum q (Å), reference stress σ_0 (GPa), and elastic modulus E (GPa). The empirical equations, fitting parameters, and goodness of fit (R^2) are denoted, and may be used to predict the strength and toughness of future 2DMs. Input data is taken from Table 1.

concentration model with the fracture simulations. We see that the stress concentration in 2DMs is related to fracture mechanics via the quantization-nonlinearity parameter a^*. The failure criterion for a 2DM with a defect of size a is $\sigma_f = \sigma_f^*/K_t$, which is a corollary of the unified fracture criterion in Eq. (5).

Prediction for future 2DMs. The unified fracture criterion presented in Eqs. (4) and (5) requires the knowledge of the nonlinear elastic parameters (E, σ_0 and n) and the quantization parameter (q). In addition, it requires the parameters J_{Ic} (or K_{Ic}) and h_1 (or k in Eq. (6)), which are obtained by fitting the MD simulation of fracture in defected 2DMs. However, future 2DMs may not be accessible for an extensive study of fracture failure in a wide range of defect lengths, as done in the current study. The question arises whether it is possible to provide reasonable predictions for the latter parameters, based on the nonlinearity and quantization parameters. It is noted that obtaining the parameter h_1 from standard tables[36] is not accurate because these tables were developed for bulk, continuum materials and do not account for quantization, and therefore are not suitable for 2DMs. Furthermore, the parameter p requires the knowledge of J_{Ic} or K_{Ic}, which, for a newly studied material, might be unknown as well.

In the following, we present an empirical approach for estimating the pristine strength σ_f^* and fracture toughness K_{Ic}, and derive the nonlinearity parameter p from them. Other approaches are possible, and might be the subject of future research. We find that q is a key parameter because it reflects the 2DM's cell size and specifically the size of the covalent bond between the atoms, a variable that affects the bond stiffness and energy. We also know that the pristine strength is roughly proportional to the reference stress σ_0 (Eq. (10) and Table 1); in plastic materials σ_0 typically marks the yield strength, but, as 2DMs are brittle materials, σ_0 marks instead an upper bound for the strength. Furthermore, we know that the fracture toughness is proportional to the square root of the modulus E. Putting these relations together, the predictions for the strength and toughness are presented in Fig. 9. We see that both the pristine strength and fracture toughness improve (increase) when the fracture quantum q is smaller, that is the 2DM cell size and bond length are smaller. In other words, a tighter atomic structure has higher strength and fracture resistance.

Based on these estimates, the prediction for p may be obtained by substituting the empirical equations for σ_f^* (or using σ_u directly from a stress-strain simulation) and K_{Ic} into Eq. (8), given that q is known from the 2DM's structural architecture. Alternatively, the nonlinearity-quantization parameter can be derived directly from Eq. (8), $a^* \cong (K_{IC}/\sigma_f^*)^2/\pi$. Once σ_f^* and a^* are known, the material fracture behavior is completely defined, as expressed by Eq. (9) and Fig. 8.

Material resistance to crack propagation

The crack driving force is expressed by J in Eq. (3) as a function of the applied stress and defect length. The material resistance, $J_R = J(\sigma_f, a)$, is obtained by substituting the fracture data-pairs $[\sigma_f, a]$ obtained by the MD analysis of each material. The crack driving force and the material resistance are depicted in Fig. 10 and Fig. S6 for the studied materials. We observe that, for each of the studied materials, the resistance curve is fairly constant with respect to defect length, even for small defects, and equals J_{Ic}. This is the signature of brittle materials, in which the fracture energy is dominated by the energy to dissociate the covalent bonds. In other words, when a defect advances by breaking a single bond, the energy released is the bonding energy, which is constant (on average). This is consistent with the analysis presented earlier. By contrast, in plastic materials, atoms tend to rearrange and rebond around the crack tip, absorbing much of the released energy.

For crack growth to be unstable, the rate of change of the driving force with respect to crack length should be higher than that of the resistance, that is, $\partial J/\partial a > \partial J_R/\partial a$ [20,36]. As $\partial J_R/\partial a \cong 0$ for all defect lengths, this condition is met when the driving force intersects the resistance curve at the smallest possible defect. For example, in graphene (Fig. 10a), this condition is met for an applied stress of $\sigma \cong 102$ GPa; a higher applied stress, for a defect of any initial length, will result in continuous crack propagation until failure. Under a lower applied stress, the defect will not propagate if its initial length is below the intersection between J_R and J, while it will propagate to failure when the initial length is above the intersection point. For example, for an applied stress of $\sigma = 60$ GPa, the graphene armchair resistance is intersected at a defect half-length of about 6 Å; for a shorter initial length, the defect will not propagate and will therefore be stable; for a longer initial length, the defect will propagate as a crack until failure and will therefore be unstable.

Comparison to other materials

By applying the UFM model to simulated fracture data of four representative brittle 2DMs as well as Ti_2C MXene from previous work, we extracted a series of fracture mechanics parameters, as listed in Table 1. Among them, the fracture toughness K_{Ic} serves as a key indicator (along with a^*) for comparing fracture resistance across different materials. The K_{Ic} values for the five 2DMs considered in this study range from approximately 0.85 to 3.00 MPa m$^{0.5}$, all within the typical range for brittle materials. Specifically, graphene (2.65–3.00 MPa m$^{0.5}$) and h-BN (2.24–2.52 MPa m$^{0.5}$)

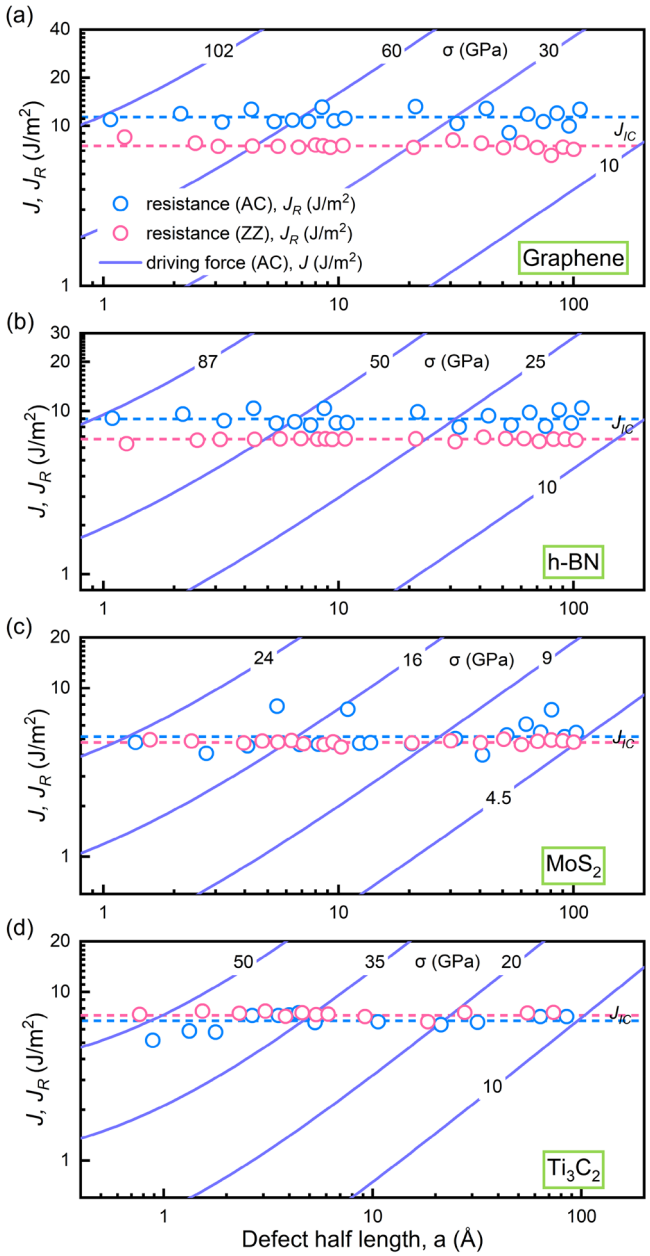

Fig. 10 | Crack instability analysis. Log-log plots of J_R resistance curves for armchair and zigzag defected models, using the material and fracture data from the MD simulations (Fig. 6 and Table 1). Panels: **a** graphene, **b** h-BN, **c** MoS_2 and **d** Ti_3C_2. J driving force curves for armchair defects for four values of the applied far-field stress σ (Eq. (3)). The critical energy release rates J_{Ic} are denoted. To avoid crack propagation, the crack length must be below the intersection between the driving force and the material resistance.

exhibit relatively high fracture toughness, approaching the lower bounds of traditional ceramics such as SiC (3–4 MPa m$^{0.5}$) and Al_2O_3 (3–5 MPa m$^{0.5}$), classifying them as low-end ceramic-like brittle materials. Ti_2C and Ti_3C_2 MXene (1.68–1.85 MPa m$^{0.5}$) display moderately lower toughness, comparable to glass ceramics (1.4–1.7 MPa m$^{0.5}$), and fall between typical soda-lime glass (0.7–0.9 MPa m$^{0.5}$) and weaker ceramics like MgO (approximately 3 MPa m$^{0.5}$), thus categorized as moderately brittle materials. MoS_2 exhibits the lowest toughness (approximately 0.85 MPa m$^{0.5}$), similar to that of ordinary glass[40,41].

Extensive experimental and computational studies have reported LEFM-based fracture toughness for long-crack cases in 2DMs. For instance, graphene[9,15,16] shows values around 3.15–4 MPa m$^{0.5}$, while MoS_2[12,18,42] falls in the range of 0.64–0.81 MPa m$^{0.5}$, similar to the values obtained in the current study. However, fracture toughness data for MXenes remains scarce, with only a few reports confirming brittle failure behavior in monolayer MXene experimentally[43]. Notably, recent experiments have shown that monolayer h-BN exhibits a surprisingly high fracture toughness (mean value approximately 8.7 MPa m$^{0.5}$), far exceeding both Griffith predictions and experimental values for graphene[9,44]. This enhancement is attributed to asymmetric elasticity and pronounced edge energy anisotropy at the crack tip, which promote frequent crack deflection and branching, increasing energy dissipation. Computational studies further confirm that monolayer materials with asymmetric lattice geometry and strong edge energy anisotropy tend to suppress unstable crack growth, leading to higher effective toughness[45].

However, it should be noted that in the present work, the empirical Tersoff potential was used for h-BN, where the bond-breaking process is primarily governed by cutting off unphysical hardening under large deformations. As a result, its ability to capture structural responses such as crack deflection and branching induced by strong edge energy anisotropy is inherently limited. Furthermore, the UFM model developed in this work describes only the critical condition for crack instability and may therefore underestimate the actual toughness in materials where toughening mechanisms such as deflection or branching occur. To overcome the above limitations and better reproduce the experimentally observed crack evolution behavior, future research should focus on developing high-precision deep learning interatomic potentials and extending new theoretical frameworks to accurately describe bond breaking and direction-dependent fracture processes in two-dimensional materials.

Conclusion

In this study, we systematically investigated the fracture behavior of five representative brittle two-dimensional materials (2DMs) with center pre-existing cracks under mode I loading, using a combined approach of molecular dynamics (MD) simulations and theoretical fracture mechanics. Based on the principle of energy balance at the atomic scale, we developed a Unified Fracture Mechanics (UFM) criterion, capable of accurately predicting the fracture strength and crack instability of brittle 2DMs at the nanoscale.

The UFM model extends classical Linear Elastic Fracture Mechanics (LEFM) by incorporating two fundamental mechanisms: nonlinear elastic response and atomic-scale structural discreteness. Our findings reveal that LEFM significantly overestimates the fracture strength in the presence of short defects. While models considering only nonlinear elasticity (NLFM) or energy quantization (QFM) offer improved predictions over LEFM, they remain insufficient for fully capturing nanoscale fracture behavior in 2DMs. In contrast, the UFM model, by coupling both nonlinearity and quantization, provides a unified and accurate description of brittle fracture across different defect length scales. It also derives the pristine strength, a known deficiency of LEFM.

Furthermore, we derived a highly-accurate analytical approximation of the UFM criterion, in which the combined effects are encapsulated in a nonlinearity–quantization parameter a^*, added to the crack half-length a. With knowledge of the pristine strength and the corresponding a^* for any given brittle monolayer 2DM, the fracture behavior of defected structures can be accurately predicted. The parameter a^* can be estimated using the empirical method proposed in this study.

Additionally, the UFM framework reveals that the resistance curves of brittle 2DMs remain nearly constant across all defect sizes, highlighting their intrinsically brittle nature. In summary, this study not only establishes a unified theoretical framework for understanding the fracture behavior of 2DMs at the atomic scale, but also provides a theoretical foundation for the mechanical reliability design and engineering applications of 2DM-based nanoscale devices. Further research is anticipated for extending this theoretical framework by incorporating more complex defect types, diverse loading conditions, as well as temperature and environmental effects. These developments should be complemented by experimental observations

across various two-dimensional material systems to validate the accuracy and applicability of the theoretical predictions.

Data availability

The data that support the findings of this study are available from the authors upon request.

Received: 16 September 2025; Accepted: 16 November 2025;
Published online: 09 January 2026

References

1. Li, X. D. et al. Resistive memory devices at the thinnest limit: progress and challenges. *Adv. Mater.* **36**, 2307951 (2024).
2. Pomerantseva, E. & Gogotsi, Y. Two-dimensional heterostructures for energy storage. *Nat. Energy* **2**, 17089 (2017).
3. Sun, X. et al. Recent progress in graphene/polymer nanocomposites. *Adv. Mater.* **33**, 2001105 (2021).
4. Wang, S. et al. Atomically sharp crack tips in monolayer MoS2 and their enhanced toughness by vacancy defects. *ACS Nano* **10**, 9831–9839 (2016).
5. Ma, Y. et al. Atomic fracture mechanism in suspended 2D transition metal dichalcogenides. *Adv. Funct. Mater.* **34**, 2409839 (2024).
6. Akinwande, D. et al. A review on mechanics and mechanical properties of 2D materials—Graphene and beyond. *Extrem. Mech. Lett.* **13**, 42–77 (2017).
7. Zheng, X. D. Twist-assisted intrinsic toughening in two-dimensional transition metal dichalcogenides. *Nat. Mater.* **24**, 1561–1568 (2025).
8. Song, Z. et al. Flaw-size-dependent mechanical interlayer coupling and edge-reconstruction embrittlement in van der Waals materials. *Nat. Mater.* **24**, 1554–1560 (2025).
9. Zhang, P. et al. Fracture toughness of graphene. *Nat. Commun.* **5**, 3782 (2014).
10. Huang, L. et al. In situ scanning transmission electron microscopy observations of fracture at the atomic scale. *Phys. Rev. Lett.* **125**, 246102 (2020).
11. Fang, Q. et al. Strong and flaw-insensitive two-dimensional covalent organic frameworks. *Matter* **4**, 1017–1028 (2021).
12. Zhang, X. et al. Atomistic measurement and modeling of intrinsic fracture toughness of two-dimensional materials. *Proc. Natl. Acad. Sci. U.S.A.* **119**, e2206756119 (2022).
13. Khare, R. et al. Coupled quantum mechanical/molecular mechanical modeling of the fracture of defective carbon nanotubes and graphene sheets. *Phys. Rev. B* **75**, 075412 (2007).
14. Yin, H. et al. Griffith criterion for brittle fracture in graphene. *Nano Lett.* **15**, 1918–1924 (2015).
15. Wang, J., Ye, X., Yang, X., Liu, M. & Li, X. The applicability and the low limit of the classical fracture theory at nanoscale: The fracture of graphene. *Eng. Fract. Mech.* **284**, 109282 (2023).
16. Shimada, T. et al. Beyond conventional nonlinear fracture mechanics in graphene nanoribbons. *Nanoscale* **12**, 18363–18370 (2020).
17. Pan, F., Tian, H. & Zhang, B. Nanofracture of stretched hexagonal boron nitride strip with an edge crack. *Eng. Fract. Mech.* **242**, 107485 (2021).
18. Elapolu, M. S. R., Tabarraei, A., Wang, X. N. & Spearot, D. E. Fracture mechanics of multi-layer molybdenum disulfide. *Eng. Fract. Mech.* **212**, 1–12 (2019).
19. Jia, P. F. et al. A unified atomic energy release rate criterion for nonlinear brittle fracture in graphene nanoribbons. *Int. J. Solids Struct.* **234**, 111260 (2022).
20. Greenfeld, I., Jiang, S. D., Yang, L. & Wagner, H. D. Nonlinear elasticity degrades monolayer fracture toughness. *Acta Mater.* **286**, 120727 (2025).
21. Pugno, N., Carpinteri, A., Ippolito, M., Mattoni, A. & Colombo, L. Atomistic fracture: QFM vs. MD. *Eng. Fract. Mech.* **75**, 1794–1803 (2008).
22. Thompson, A. P. et al. LAMMPS-a flexible simulation tool for particle-based materials modeling at the atomic, meso, and continuum scales. *Comput. Phys. Commun.* **271**, 108171 (2022).
23. Rao, C. N. R., Sood, A. K., Subrahmanyam, K. S. & Govindaraj, A. Graphene: the new two-dimensional nanomaterial. *Angew. Chem. Int. Ed.* **48**, 7752–7777 (2009).
24. Roy, S. et al. Structure, properties and applications of two-dimensional hexagonal boron nitride. *Adv. Mater.* **33**, 2101589 (2021).
25. Xu, M. S., Liang, T., Shi, M. M. & Chen, H. Z. Graphene-like two-dimensional materials. *Chem. Rev.* **113**, 3766–3798 (2013).
26. VahidMohammadi, A., Rosen, J. & Gogotsi, Y. The world of two-dimensional carbides and nitrides (MXenes). *Science* **372**, eabf1581 (2021).
27. Stuart, S. J., Tutein, A. B. & Harrison, J. A. A reactive potential for hydrocarbons with intermolecular interactions. *J. Chem. Phys.* **112**, 6472–6486 (2000).
28. Los, J. H. et al. Extended Tersoff potential for boron nitride: Energetics and elastic properties of pristine and defective h-BN. *Phys. Rev. B* **96**, 184108 (2017).
29. Liang, T., Phillpot, S. R. & Sinnott, S. B. Parametrization of a reactive many-body potential for Mo-S systems. *Phys. Rev. B* **79**, 245110 (2009).
30. Osti, N. C. et al. Effect of metal ion intercalation on the structure of MXene and water dynamics on its internal surfaces. *ACS Appl. Mater. Interfaces* **8**, 8859–8863 (2016).
31. Zhang, G. et al. A unified strength criterion for two-dimensional materials via bond failure analysis. *J. Mech. Phys. Solids* **181**, 105466 (2023).
32. Wu, J. Y. et al. Grain-size-controlled mechanical properties of polycrystalline monolayer MoS_2. *Nano Lett.* **18**, 1543–1552 (2018).
33. Jiang, S. D. et al. Fracture mechanisms and crack propagation in monolayer $Ti_3C_2T_x$ under nanoindentation: the influence of surface terminations and vacancy defects. *ACS Appl. Mater. Interfaces* **16**, 48113–48125 (2024).
34. Pugno, N. M. & Ruoff, R. S. Quantized fracture mechanics. *Philos. Mag.* **84**, 2829–2845 (2004).
35. Ramberg, W., William, R. S. *Description of Stress-Strain Curves by Three Parameters* (National Advisory Committee for Aeronatics, 1943).
36. Anderson, T. L. *Fracture Mechanics Fundamentals and Applications* 4th edn. (CRC Press, 2017).
37. Kumar, V., German, M. D., Shih, C. F. An engineering approach for elastic-plastic fracture analysis. in *EPRI Project*. (General Electric Company, 1981).
38. Inglis, C. E. Stresses in a plate due to the presence of cracks and sharp corners. *Trans. Inst. Nav. Archit.* **55**, 219–241 (1913).
39. Pilkey, W. D. *Peterson's Stress Concentration Factors*, 2nd edn (John Wiley & Sons, Inc., 1997).
40. Ashby, M. F. *Materials Selection in Mechanical Design* 4th edn. (Elsevier, 2011).
41. Meyers, M. A., Chawla, K. K. *Mechanical Behavior of Materials* (Cambridge University Press, 2008).
42. Yang, Y. C. et al. Brittle fracture of 2D $MoSe_2$. *Adv. Mater.* **29**, 1604201 (2017).
43. Rong, C. et al. Elastic properties and tensile strength of 2D $Ti_3C_2T_x$ MXene monolayers. *Nat. Commun.* **15**, 1566 (2024).
44. Yang, Y. et al. Intrinsic toughening and stable crack propagation in hexagonal boron nitride. *Nature* **594**, 57–61 (2021).
45. Yu, M. L., Zhao, Z. Q., Guo, W. L. & Zhang, Z. H. Fracture toughness of two-dimensional materials dominated by edge energy anisotropy. *J. Mech. Phys. Solids* **186**, 105579 (2024).

Acknowledgements

Lin Yang extends his gratitude to Daniel Wagner from the Weizmann Institute of Science and Liyong Tong from the University of Sydney for their invaluable

guidance. He also appreciates the inspiration gained from his research experience at the Weizmann Institute of Science. Israel Greenfeld and H. Daniel Wagner would like to acknowledge support from the G.M.J. Schmidt Minerva Center of Supramolecular Architectures at the Weizmann Institute, and the generosity of the Harold Perlman family. This work is supported by the Science Foundation of National Key Laboratory of Science and Technology on Advanced Composites in Special Environments, Harbin Institute of Technology (Grant No.6142905243606).

Author contributions

S.J. conceived the original idea and framework and performed the molecular dynamics simulations. I.G. developed the fracture mechanics model. S.J. and I.G. jointly wrote the first draft of the manuscript and conducted data analysis. W.Y. and X.H. assisted with data analysis and discussion of the results. L.Y. and H.D.W. revised and finalized the manuscript. All authors discussed the results and approved the final version of the manuscript.

Competing interests

The authors declare no competing interests.

Additional information

Supplementary information The online version contains supplementary material available at https://doi.org/10.1038/s41524-025-01868-z.

Correspondence and requests for materials should be addressed to Lin Yang or H. Daniel Wagner.